Targeting of microvillus protein Eps8 by the NleH effector kinases from enteropathogenic *E. coli*

Georgina L. Pollock[a,b,c] (ID), Andrey M. Grishin[d], Cristina Giogha[a,b] (ID), Jiyao Gan[a,b] (ID), Clare V. Oates[c] (ID), Paul J. McMillan[e,1], Isabella Gaeta[f],
Matthew J. Tyska[f] (ID), Jaclyn S. Pearson[a,b,g], Nichollas E. Scott[c] (ID), Miroslaw Cygler[d,2], and Elizabeth L. Hartland[a,b,c,g,2] (ID)

Attaching and effacing (AE) lesion formation on enterocytes by enteropathogenic *Escherichia coli* (EPEC) requires the EPEC type III secretion system (T3SS). Two T3SS effectors injected into the host cell during infection are the atypical kinases, NleH1 and NleH2. However, the host targets of NleH1 and NleH2 kinase activity during infection have not been reported. Here phosphoproteomics identified Ser775 in the microvillus protein Eps8 as a bona fide target of NleH1 and NleH2 phosphorylation. Both kinases interacted with Eps8 through previously unrecognized, noncanonical "proline-rich" motifs, PxxDY, that bound the Src Homology 3 (SH3) domain of Eps8. Structural analysis of the Eps8 SH3 domain bound to a peptide containing one of the proline-rich motifs from NleH showed that the N-terminal part of the peptide adopts a type II polyproline helix, and its C-terminal "DY" segment makes multiple contacts with the SH3 domain. Ser775 phosphorylation by NleH1 or NleH2 hindered Eps8 bundling activity and drove dispersal of Eps8 from the AE lesion during EPEC infection. This finding suggested that NleH1 and NleH2 altered the cellular localization of Eps8 and the cytoskeletal composition of AE lesions during EPEC infection.

T3SS | kinase | microvillus | Eps8 | EPEC

The enteric pathogen enteropathogenic *Escherichia coli* (EPEC) is a causative agent of diarrheal disease predominantly in infants under 2 years of age (1). EPEC infects enterocytes in the small intestine and forms characteristic lesions on the apical surface known as attaching and effacing (AE) lesions. The defining features of AE lesions are intimate attachment of the bacteria to the host cell, loss of microvilli at the site of bacterial attachment, elongation of adjacent microvilli, and accumulation of filamentous actin beneath the site of bacterial attachment (2).

AE lesion formation and EPEC pathogenicity require a bacterial type III secretion system (T3SS), which translocates 25–30 effectors into the host enterocyte during infection, two of which are NleH1 and NleH2 (3). Homologs are found in other AE pathogens, including enterohemorrhagic *E. coli* and *Citrobacter rodentium*. NleH effectors possess a C-terminal kinase domain including a class I PSD-95/Disk Large/ZO-1 binding motif, while the N terminus appears to be intrinsically disordered (4, 5). NleH1 and NleH2 have been implicated in the inhibition of both innate inflammatory and cell death signaling pathways and have been variously reported to bind directly to ribosomal protein s3, the v-Crk sarcoma virus CT10 oncogene-like protein, and the cell death suppressor Bax-inhibitor 1 (6–11). However, the host targets phosphorylated by NleH1 and NleH2 during EPEC infection have not been identified to date (12). In this study, we performed phosphoproteomics on EPEC-infected cells to determine that NleH1 and NleH2 target Ser775 in the microvillus protein Eps8 for phosphorylation. Ser775 was essential for the bundling activity of Eps8, and in the absence of NleH1 and NleH2, Eps8 was retained in the AE lesion during EPEC infection. This suggested that NleH1 and NleH2 alter the cytoskeletal composition of AE lesions.

Results and Discussion

Role of NleH Kinases in Inflammation and Cell Death Inhibition. Initially to interrogate the mechanism by which NleH1 and NleH2 modulated inflammatory and cell death signaling pathways, we sought to confirm previously published reports that NleH1 and NleH2 inhibited IκBα degradation in response to inflammatory stimuli, thereby suppressing NF-κB-dependent transcription (7–11). Using HeLa cell lines virally transduced to express either NleH1 or NleH2, we found that neither NleH1 nor NleH2 inhibited tumor necrosis factor–induced IκBα degradation as previously reported, nor did we observe any role for NleH1 or NleH2 in the enhancement or suppression of

NF-κB-dependent luciferase reporter activity in transient transfection (*SI Appendix*, Fig. S1 *A and B*). Furthermore, HeLa cells infected with an EPEC E2348/69 derivative lacking both *nleH* genes (Δ*nleH1*Δ*nleH2*) were protected from tumor necrosis factor–induced IκBα degradation similar to cells infected with wild-type EPEC, whereas Δ*escN*, lacking a functional T3SS, and Δ*nleE*, lacking a known inhibitor of NF-κB activation, were unable to block IκBα degradation (*SI Appendix*, Fig. S1*C*). NleH1 has previously been reported to inhibit caspase-3 cleavage in cells treated with a variety of cytotoxic compounds, including staurosporine, brefeldin A, tunicamycin, and *Clostridium difficile* toxin B (6, 13). Again, using virally transduced HeLa cell lines, we observed that neither NleH1 nor NleH2 expression inhibited caspase-8 or -3 cleavage in cells treated with proapoptotic stimuli FasL or staurosporine, respectively (*SI Appendix*, Fig. S1 *D and E*).

Eps8 Is a Substrate of NleH. Given that we could not reproduce a role for NleH1 or NleH2 in cell death or inflammatory

signaling, we undertook an unbiased approach to identify putative substrates of NleH1 and NleH2 kinase activity. To this end, we conducted a label-free quantitative phosphoproteomic comparison of uninfected HT-29 intestinal cells with HT-29 intestinal cells infected with wild-type EPEC E2348/69, Δ*nleH1*Δ*nleH2*, or Δ*nleH1*Δ*nleH2* complemented with plasmids expressing either NleH1 or NleH2. Titanium dioxide–based phosphopeptide enrichment resulted in the identification of 11,292 phosphorylation sites, of which 6,865 corresponded to class I phosphorylation sites (sites with a localization probability of >0.75), which were considered for further analysis. Comparison of cells infected with EPEC E2348/69 and Δ*nleH1*Δ*nleH2* revealed multiple phosphorylation sites from wild-type infection that showed a >16 fold (4 log^2) change with a *P* value <0.001 that were considered as putative substrates (Fig. 1*A*, PRIDE accession PXD008480). Within the most differentially phosphorylated targets, members of the Eps8 protein family including Eps8 (Ser775), Eps8L1 (Ser621), and Eps8L2
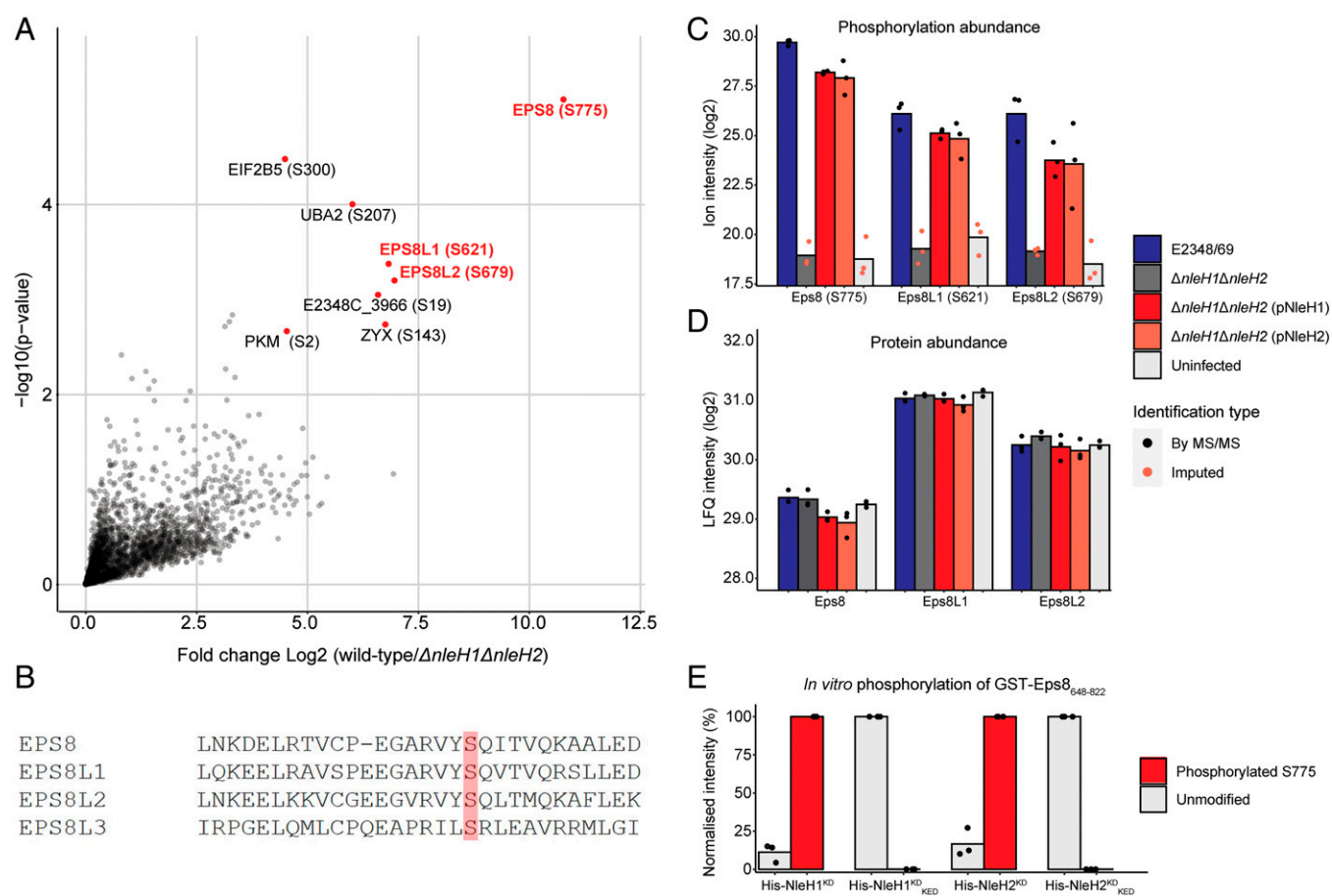

Fig. 1. Phosphorylation of Eps8 family proteins by NleH1 and NleH2. *A.* Phosphoproteomics was performed on HT-29 cells infected with wild-type EPEC E2348/69 for 3 h and compared to cells infected with the Δ*nleH1*Δ*nleH2* double mutant. Scatter plot of class I phosphorylation sites shows the mean ion intensity ratios of HT-29 cells infected with EPEC E2348/69 compared to cells infected with Δ*nleH1*Δ*nleH2* and are plotted against the –log10 (*P* value) derived from a Student's *t* test. Gray dots represent identified phosphorylation sites. Phosphorylation events with a ≥16-fold change in abundance in E2348/69-infected cells compared to cells infected with Δ*nleH1*Δ*nleH2*, with *P* < 0.01, are represented by red dots. Phosphorylation sites of interest are labeled with the corresponding gene name and phosphorylated residue shown in parentheses. *B.* Amino acid sequence alignment of segments of Eps8 family proteins, with the serine residue phosphorylated by NleH shown in red. *C.* Bar plots of Eps8 S775, Eps8L1 S621, and Eps8L2 S679 phosphorylation events within uninfected HT-29 cells or cells infected with wild-type EPEC E2348/69, Δ*nleH1*Δ*nleH2* double mutant, or Δ*nleH1*Δ*nleH2* complemented with plasmids expressing either NleH1 (pNleH1) or NleH2 (pNleH2) for 3 h. The mean ion intensities for each condition are plotted as bar plots, with individual measurements from each biological replicate plotted as dots. Black dots represent ion intensities from phosphorylation events identified by MS/MS within a biological replicate, while pink dots represent imputed values. *D.* Bar plots of Eps8, Eps8L1, and Eps8L2 protein abundances within uninfected HT-29 cells or cells infected with wild-type EPEC E2348/69, Δ*nleH1*Δ*nleH2* double mutant, or Δ*nleH1*Δ*nleH2* complemented with pNleH1 or pNleH2 for 3 h. The mean LFQ ion intensities for each condition are plotted as bar plots, with individual measurements from each biological replicate plotted as dots. Black dots denote LFQ ion intensities derived from MS/MS information within each biological replicate. *E.* Normalized ion intensities of the peptide forms of VYSQITVQK identified within recombinant GST-Eps8$_{648-822}$ incubated for 3 h with the kinase domains of NleH1 (His-NleH1^{KD}) and NleH2 (His-NleH2^{KD}) and their respective active site mutants (His-NleH1$^{KD}_{KED}$ and His-NleH2$^{KD}_{KED}$). Results are shown as relative percentages with ion intensities normalized to the most abundant peptide form identified in each condition. Black dots represent the peptides detected in each replicate.

(Ser679), phosphorylation occurred on a common shared serine residue (Fig. 1 *A* and *B*). Phosphorylation of this serine was not observed within uninfected samples or cells infected with Δ*nleH1*Δ*nleH2* yet was restored upon complementation with *nleH1* or *nleH2* (Fig. 1*C*, and PRIDE accession PXD031090). Minimal changes to protein abundance were observed within Eps8 protein family members during infections (Fig. 1*D*, PRIDE accession PXD008481).

Eps8L2 has been previously identified as a putative substrate of NleH1 (enterohemorrhagic *E. coli* O157:H7 EDL933) kinase activity; however, this finding was not validated (11). Given that Eps8 is the most well studied of the Eps8 family members and highly expressed in intestinal tissue (14), further validation here focused only on Eps8. Direct phosphorylation of Eps8 by NleH1 and NleH2 was confirmed via an in vitro kinase assay whereby the purified effector region (residues 648–822) of Eps8 was incubated with the purified kinase domain of NleH1 or NleH2, termed NleH1^{KD} (residues 128–293) and NleH2^{KD} (residues 140–303), respectively, or their catalytically inactive counterparts, termed NleH1$^{KD}_{KED}$ and NleH2$^{KD}_{KED}$. Proteins were subjected to polyacrylamide gel electrophoresis (PAGE) and in-gel tryptic digest, followed by mass spectrometric analysis. Consistent with previous results, we observed NleH1 and NleH2 phosphorylated Eps8 at Ser775 (Fig. 1*E*, PRIDE accession PXD010925).

In Vitro Identification of Eps8 Phosphorylation Site Targeted by NleH. Eps8 has a modular domain structure consisting of a split pleckstrin homology domain (residues 69–129 and 381–414), proline-rich regions (PRRs) (aa 421–440 and 615–651), an Src Homology 3 domain (SH3) domain (aa 531–591), and an "effector" or actin binding region (aa 648–822) (15) (Fig. 2*A*). Phosphorylation of the Eps8 effector region by NleH1 and NleH2 was further examined in vitro with ATP-γS as a substrate, which introduces an artificial thiophosphate group (16) (*SI Appendix*, Fig. S2 *A* and *B*). To confirm the site of phosphorylation, derivatives of the Eps8 effector region, Eps8(648–822), carrying Ser to Ala amino acid substitutions, were created, including Ser685, Ser703, Ser775, and a stretch of serine residues $_{659}$SSSSDS$_{664}$. The resultant purified proteins were incubated with ATP-γS and NleH1^{KD} before being subjected to PAGE and immunoblot with anti–thiophosphate ester antibodies. Eps8(648–822) was phosphorylated in the presence of NleH1^{KD} and ATP-γS, as were the Eps8 alanine substituted mutants Eps8(S685A), Eps8(S703A), and Eps8($_{659}$SSSSDS$_{664}$–$_{659}$AAAADA$_{664}$). However, Eps8(S775A) was not phosphorylated by NleH1^{KD} (*SI Appendix*, Fig. S2*B*). Together these results indicate NleH catalyzes the addition of a single phosphate moiety to the Eps8 effector region, specifically to Ser775.
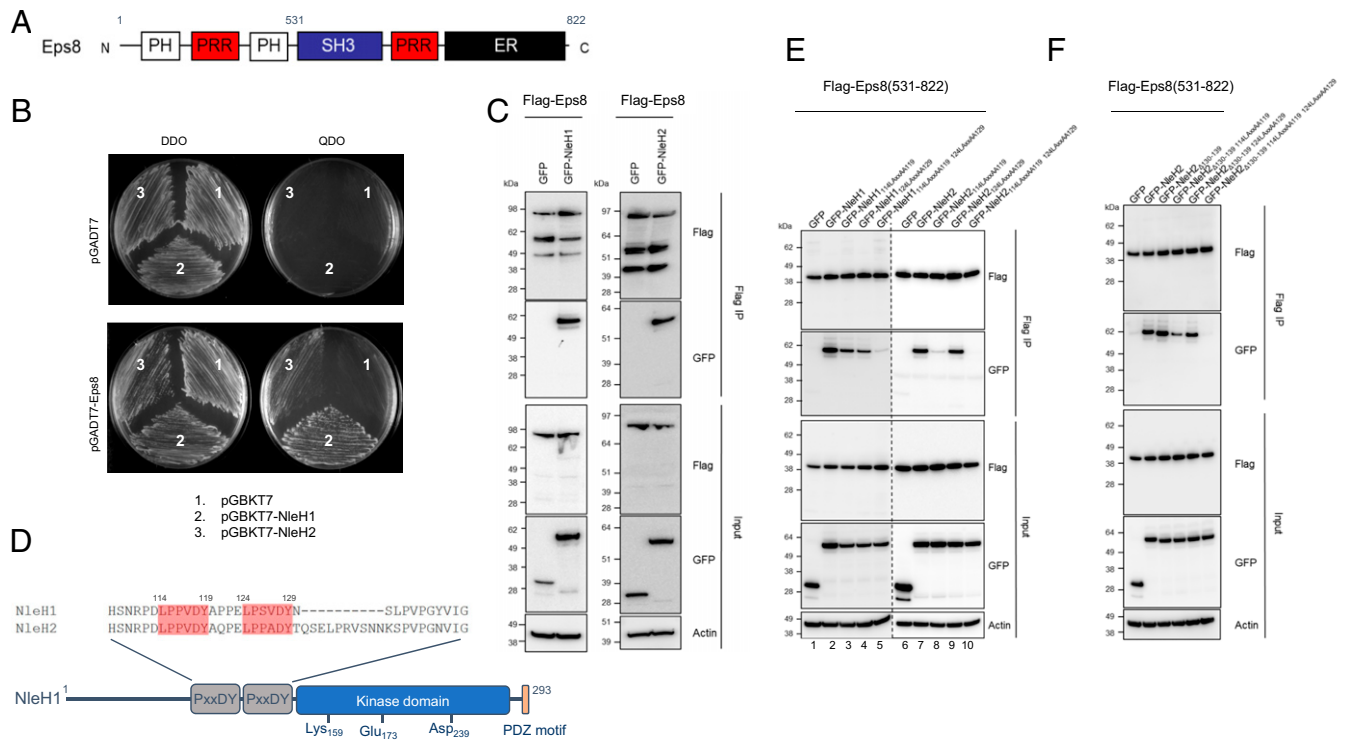

Fig. 2. Eps8–NleH interactions are mediated by noncanonical SH3 domains. *A*. Schematic representation of Eps8 modular domain structure. PH, pleckstrin homology; PRR, proline rich region; SH3, Src homology 3; ER, effector region. *B*. Yeast two-hybrid analysis of protein–protein interactions in *S. cerevisiae* PJ69-4A. Growth on selective media for plasmid maintenance (DDO, double dropout) or selective media for interaction between proteins (QDO, quadruple dropout). Interactions on QDO shown for yeast strains carrying pGADT7:Eps8 and pGBKT7:NleH1 or pGBKT7:NleH2 *C*. Immunoblot of Flag-Eps8 immunoprecipitation and detection of GFP-NleH1 and GFP-NleH2 in cotransfected HEK293T cells. Actin, loading control. Representative immunoblots from at least three independent experiments. *D*. Partial amino acid sequence alignment between NleH1 and NleH2 from EPEC E2348/69 with identified noncanonical SH3-domain binding motifs (PxxDY) shown in red and a schematic showing their position in NleH1 as well as the catalytic KED motif of NleH1 and PSD-95/Disk Large/ZO-1 (PDZ) binding motif. The amino acid sequences of NleH1 and NleH2 are identical apart from a 10-aa insertion in NleH2 shown in the partial alignment. *E*. Immunoblot of anti-FLAG immunoprecipitation in HEK293T cells cotransfected with Flag-Eps8(531–822) and GFP-NleH1 or GFP-NleH2 or the PxxDY mutant derivatives thereof. GFP fusion proteins were detected with anti-GFP antibodies, and immunoblots of input samples show protein expression levels. Actin, loading control. Representative immunoblots from at least three independent experiments. *F*. Immunoblot of anti-FLAG immunoprecipitation in HEK293T cells cotransfected with Flag-Eps8(531–822) and GFP-NleH2 or derivatives lacking amino acids 130–139. GFP fusion proteins were detected with anti-GFP antibodies, and immunoblots of input samples show protein expression levels. Actin, loading control. Representative immunoblots from at least three independent experiments.

3 of 11

NleH Binds Eps8 through a Noncanonical PRR-SH3 Motif Interaction. Using coimmunoprecipitation in HEK293T cells and a yeast two-hybrid analysis, we confirmed an interaction between Eps8 and NleH1 or NleH2 (Fig. 2 *B* and *C*). Knowing that the kinase domain of NleH1 and NleH2 phosphorylates the Eps8 effector region, we initially hypothesized that binding between NleH and Eps8 is mediated by these domains. However, no sustained interaction between the NleH2 kinase domain (140–303) and the Eps8 effector region (648–822) was detected in vitro by either size exclusion chromatography or isothermal titration calorimetry (*SI Appendix*, Fig. S2 *C* and *D*). Thus, the interaction between the NleH kinase domain and the Eps8 effector region upon phosphorylation appeared to be transient.

It was previously shown that the SH3 domain of Eps8 preferentially recognizes a noncanonical "proline-rich" motif, PxxDY (17). Scanning of the amino acid sequence of NleH1 and NleH2 identified two distinct PxxDY motifs spanning residues 114–119 and 124–129 in each protein (Fig. 2*D*). This finding suggested an interaction between the N-terminal segments of NleH1 and NleH2 and the SH3 domain of Eps8. To verify that binding of Eps8 to NleH1 and NleH2 was mediated by the SH3 domain, we performed coimmunoprecipitations in HEK293T cells expressing Eps8(531–822), encompassing the SH3, PRR, and effector region domains (Fig. 2*A*) of Eps8, and showed that this segment was able to pull down NleH1 (Fig. 2*E*, lanes 2 and 7). We then expressed and purified Eps8(531–822), NleH1(96–293), and NleH2(96–303), which in addition to the kinase domain included the two identified PxxDY motifs. When these Eps8 and NleH1 or NleH2 constructs were combined, a subsequent size exclusion chromatogram showed a shift in the peak position toward a higher molecular weight as compared to the individual constructs, with the shifted peak containing both proteins (*SI Appendix*, Fig. S3 *A* and *B*). Since each NleH contains two PxxDY motifs, we also ran size exclusion chromatography with a 2:1 molar ratio of Eps8:NleH. We observed a further shift of the peak, suggesting a possible 2:1 stoichiometry of binding (*SI Appendix*, Fig. S3*B*). The SH3 domain of Eps8 was reported to bind the E3b1 peptide PPPPPVDYEDEE with a K_d of 35 μM (17), while the Eps8L1(SH3) domain (an Eps8 homolog) bound CD3ε peptide PPVPNPDYEPIR with a K_d of 24 μM (18). The same DY-motif peptide interacted with the N-terminal Nck1 SH3 domain, with an 8.3 μM constant (19). To quantify the strength of Eps8(SH3)–NleH1/2 interactions we used isothermal titration calorimetry and measured the K_d for Eps8(531–822) binding to NleH1(96–293) and NleH2(96–303) to be 8.6 μM and 7.7 μM, respectively (*SI Appendix*, Fig. S3*C*), indicating that NleH binds Eps8 with similar affinity to endogenous binding partners of Eps8.

To further characterize the role of NleH SH3-binding motifs, we created derivatives of GFP-NleH1 where the PxxDY motifs $_{114}$LPxxDY$_{119}$ and $_{124}$LPxxDY$_{129}$ were mutated to $_{114}$LAxxAA$_{119}$ or $_{124}$LAxxAA$_{129}$. When only one of these motifs was mutated, Flag-Eps8(531–822) was able to pull down the NleH1 LPxxDY mutant (Fig. 2*E*, lanes 3 and 4). However, binding was abolished when both motifs were mutated (Fig. 2*E*, lane 5). This indicated that the binding of Eps8 and NleH1 was mediated by an SH3–LPxxDY interaction, where either one of the NleH1 LPxxDY motifs could participate. In contrast, we observed that mutation of GFP-NleH2 $_{114}$LPxxDY$_{119}$ alone abrogated binding to Flag-Eps8(531–822) (Fig. 2*E*, lane 8), indicating the first NleH2 LPxxDY motif alone conferred binding to the SH3 domain of Eps8.

Although NleH1 and NleH2 are highly homologous, NleH2 possesses a 10-aa insertion at position 130–139 that is lacking

in NleH1. The insertion is located immediately after the $_{124}$LPxxDY$_{129}$ motif and before the C-terminal kinase domain (Fig. 2*D*). We hypothesized that the 10-aa insertion may occlude the $_{124}$LPxxDY$_{129}$ SH3 binding site, explaining the different Eps8 binding profiles of NleH1 and NleH2. To test this, we constructed a derivative of GFP-NleH2 lacking residues 130–139 (NleH2$_{Δ130–139}$) and tested its ability to bind Flag-Eps8(531–822). We observed that the deletion of residues 130–139 restored the ability of NleH2$_{114LAxxAA119}$ to bind Flag-Eps8(531–822) and only upon mutation of both $_{114}$LPxxDY$_{119}$ and $_{124}$LPxxDY$_{129}$ was binding to Flag-Eps8(531–822) abolished (Fig. 2*F*).

The NleH1 and NleH2 PxxDY motif mutants were subsequently expressed in *E. coli*, purified and interrogated for binding to Eps8 by isothermal titration calorimetry, and similar results to the described above coimmunoprecipitation experiments were obtained. When only one motif was mutated, binding was still observed, but no measurable binding occurred when both SH3 binding sites were mutated (*SI Appendix*, Fig. S4 *A* and *B*). We then postulated that the interaction between the NleH kinase domain and Eps8 C-terminal effector region may strengthen the overall interaction between NleH and Eps8, mostly mediated by the SH3–PxxDY motif interactions. We determined the binding constant between just the SH3 domain Eps8(531–591) and a shorter NleH1(111–293) construct, which starts immediately at the N terminus of the first PxxDY motif. The measured K_d of 11.6 μM was similar to the K_d of 8.6 μM for NleH1(96–293) and Eps8(531–822) (*SI Appendix*, Fig. S3*C*). This result confirmed a negligible contribution of the Eps8 effector region and NleH kinase domain to the overall binding between these two proteins.

Structural analysis of the Eps8 SH3–NleH PxxDY interaction. The structure of apo Eps8 SH3 domain was previously determined by crystallography and found in either a monomeric (20) or an intertwined dimeric (21) form, depending on crystallization conditions. A complex of the Eps8L1 SH3, a homolog of Eps8, with PPVPNPDYEPIR peptide containing the PxxDY motif has been determined previously by NMR spectroscopy (18). Since the Eps8 SH3 domain can form monomers and dimers, we first examined the solution state of the recombinant SH3 domain (aa 531–591) by multiangle light scattering (*SI Appendix*, Fig. S5A). The protein eluted in a single peak with a multiangle light scattering–derived molecular weight of 7,700 Da, in good agreement with the predicted molecular weight of 7,361 Da for a monomeric form. To elucidate the molecular interactions between the Eps8 SH3 domain and the NleH PxxDY motif, we determined the structure of the Eps8 SH3 domain in complex with the peptide ^{121}PPELPSVDYNSL encompassing the second NleH1 PxxDY proline-rich motif (residues 124–129) by X-ray crystallography (*SI Appendix*, Table S1). The structures of the SH3 domain in the complex and the apo-SH3 are nearly identical and superimpose with the root-mean-square deviation of 0.6 Å for all $C^α$ atoms. Only a few sidechains undergo a rotation when the substrate binds. The Eps8 SH3 architecture adheres to the canonical SH3 fold, with a five-stranded β-barrel, three loops (RT loop, n-Src loop, and distal loop), and one short segment of a 3_{10} helix (Fig. 3 *A* and *B*). Of the peptide, eight residues (PELPSVDY) make direct contacts with the SH3 domain over a large, 560 Å^2 interface.

Key interactions are formed by the NleH1 peptide residues Pro125, Asp128, and Tyr129 (PxxDY motif) (Fig. 3 *A* and *B*). Pro125^{NleH1} interacts edgewise with hydrophobic edges of Trp567 and Pro581 of Eps8 SH3. The carboxyl group of
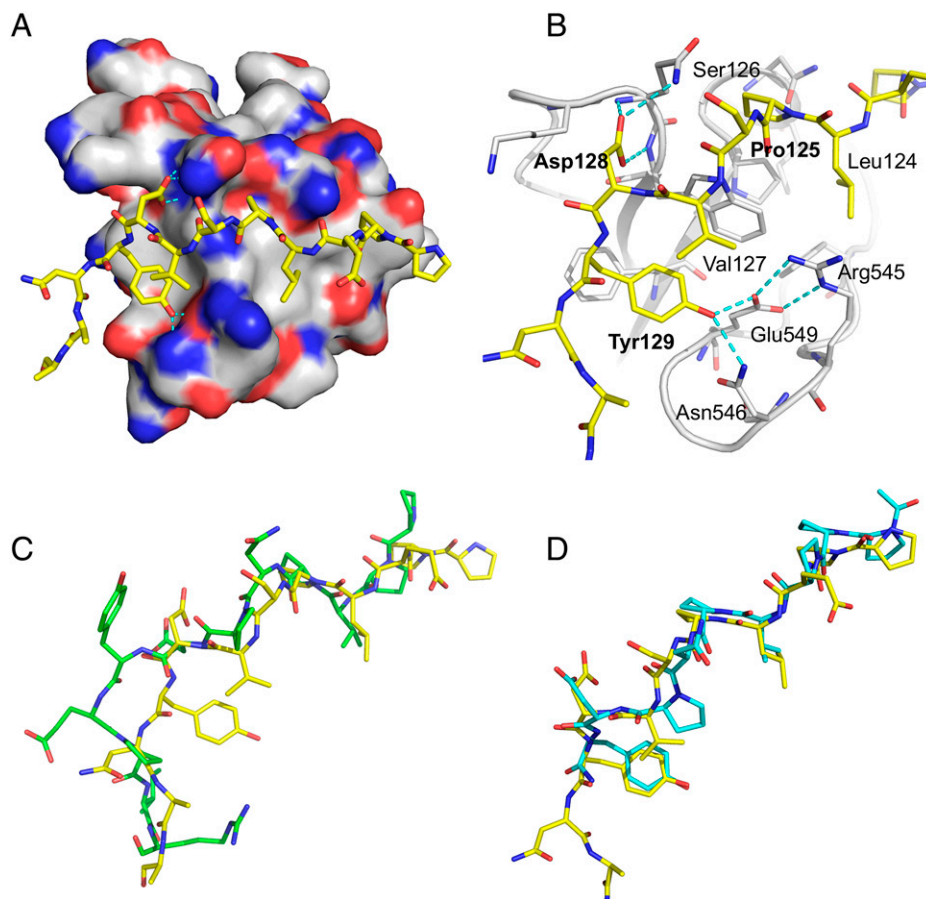
Fig. 3. Crystal structure of Eps8 SH3 domain with the NleH PPELPSVDYNSL peptide. *A*. The PxxDY peptide binds in a shallow canyon on SH3 surface. The SH3 surface is colored by atom type: N, blue; O, red; C, white. The peptide is shown in a stick mode with the C atoms colored yellow. The charge and spatial complementarity between the SH3 domain and the NleH1 peptide is visible. Cyan dashed lines indicate hydrogen bonds. *B*. Closeup of the peptide–SH3 contacts. Asp and Tyr sidechains form hydrogen bonds (dashed lines) to the sidechain and mainchain atoms of SH3 residues. The P, D, and Y residues of the PxxDY motif are labeled in bold. *C*. PxxDY peptide bound to Eps8L1 SH3 (NMR structure 2ROL, green carbons) and NleH peptide bound to Eps8 SH3 (this structure, yellow carbons) based on the superposed SH3 domains. The key tyrosine points in different directions in the two structures *D*. PxxDY peptides from Nck1 (X-ray structure 5QU2, green carbons) and Eps8 SH3 domains (this structure, yellow carbons) based on the superposition of the corresponding SH3 domains. The conformations of these two peptides are very similar despite several amino acid differences.

Asp128[NleH1] sidechain forms hydrogen bonds with the mainchain amide groups of Gln566 and Trp567 and the Gln566 N$^\varepsilon$ sidechain atom of Eps8. These two residues are located at the beginning of the n-Src loop. The amino group of the Lys565 of Eps8 SH3, located 5.7 Å from the carboxylate of Asp128[NleH1], provides additional electrostatic interactions. The Tyr129[NleH1] sidechain interacts with an SH3 hydrophobic pocket formed by the sidechains of Phe579 and Trp567 of Eps8 SH3. Moreover, the Tyr129[NleH1] hydroxyl is hydrogen-bonded to the primary amide group of Asn546 sidechain and the carboxyl group of Glu549 sidechain in Eps8 SH3, the latter also involved in a salt bridge with Arg545. The hydroxy group of Tyr129[NleH1] is so tightly surrounded by the sidechains of Glu549, Arg545, and Asn546 of Eps8 SH3 that the phosphorylation of this Tyr in each of the PxxDY NleH motifs should disrupt the binding with the Eps8 SH3 domain, as can be seen for the CD3ε peptide and the SH3 domains of Nck1 and Eps8L1 (22). However, we did not observe phosphorylation of tyrosine in any of the NleH PxxDY motifs in our mass spectrometry (MS) data. Additionally, Leu124[NleH1] fits into a hydrophobic pocket formed by Trp567, Pro581, Phe542, and Leu584 of Eps8 SH3. The mainchain carbonyl of Glu123[NleH1] forms a hydrogen bond with the mainchain amide group of Asn583[Eps8]. Finally, Pro121[NleH1] and Pro122[NleH1] participated in hydrophobic interactions with Tyr540 of Eps8 SH3. The

N-terminal peptide residues PPELP, preceding the DY motif, form a polyproline helix, type II, characteristic of a class II SH3 ligand (*SI Appendix,* Fig. S5*B*).

The observed conformation of the peptide in our structure differs in two aspects from the conformation of the PPVPNPDYE-PIR peptide bound to Eps8L1 SH3 as determined by NMR (Fig. 3*C*) (18). First, the Tyr sidechain in the DY motif near the C terminus is turned away from the SH3 and makes partial stacking interactions with Arg512 of the Eps8L1 sidechain. Moreover, the sidechain of the DY Asp residue in that structure, while pointing toward SH3, does not make hydrogen bonds with the SH3 residues as observed in our structure. These differences, however, may be artifacts of the NMR signal broadening for this Tyr residue, so the refining proceeded without intermolecular and intramolecular distance restraints involving this residue. Second, the N-terminal PPV(P) residues, preceding the PxxDY motif, did not form a type II polyproline helix, being restricted to superficial contacts with Asn530 and Ile531 of Eps8L1.

The interaction of the noncanonical "proline-rich" PxxDY motif with other SH3 domains was studied previously by NMR for the SH3 domain of Nck2 (2JBX) (23) and by crystallography for Nck1 (5QU2, 1 Å resolution) (19). The peptide conformation and peptide–SH3 contacts are similar in the two Nck structures except for the orientation of the Asp sidechain that in the NMR structure is turned away from SH3. This may

also be the result of the lack of NOE restraints involving this sidechain. The conformation of the peptide and sidechain interactions with Eps8 SH3 domain in our structure are very similar to those observed in Nck1 structures complexed with the PPPVPNPDY peptide, despite five amino acid differences in the peptide interacting surface between Eps8 and Nck1 SH3 domains, namely Phe542 in Eps8 is Tyr in Nck1, Arg545 is Gln, Ser548 is Gln, Glu566 is Ser, and Ile584 is Tyr (Fig. 3D).

Impact of NleH Phosphorylation on Eps8 Bundling and Subcellular Distribution. Eps8 is a dual function actin capping and bundling protein that is required for correct morphogenesis of intestinal microvilli. Eps8 bundling activity, rather than capping activity, is purportedly more important for microvillus morphogenesis (24–26). The C-terminal effector region of Eps8 has two structurally distinct actin capping (aa 679–697) and actin bundling domains (aa 717–784) (27), and loss of Eps8 results in microvillus shortening in both polarized epithelial cell models and the mouse intestine (28, 29). Given that Ser775 lies in the actin bundling region of Eps8 and

microvillus perturbations are a defining feature of EPEC AE lesions, we sought to investigate whether phosphorylation of Eps8 Ser775 by NleH1 and NleH2 disrupted the actin bundling activity of Eps8. Consistent with published observations, overexpression of Eps8 (as GFP-Eps8) in nonpolarized HEK293T cells led to the formation of Eps8 bundles and actin cables (24, 30), whereas coexpression of GFP-Eps8 with mCherry-NleH1 or -NleH2 disrupted Eps8 bundle formation (Fig. 4 A and B). In this overexpression system, restoration of Eps8 bundling required mutation of not only the KED catalytic triad but also both PxxDY motifs in NleH1 and NleH2 (*SI Appendix*, Fig. S6).

As expected, a bundling deficient mutant of Eps8 (Eps8$_{LNK}$ (27)) was unable to induce the formation of actin bundles (Fig. 4 C and D), and consistently, derivatives of GFP-Eps8 where Ser775 was substituted with alanine to remove the phosphorylation site (Eps8$_{S775A}$) or with aspartic acid (Eps8$_{S775D}$) to mimic Ser775 phosphorylation by NleH1 and NleH2 showed significantly diminished bundling activity (Fig. 4 C and D). Interestingly, Eps8 carrying the S775A mutation retained some
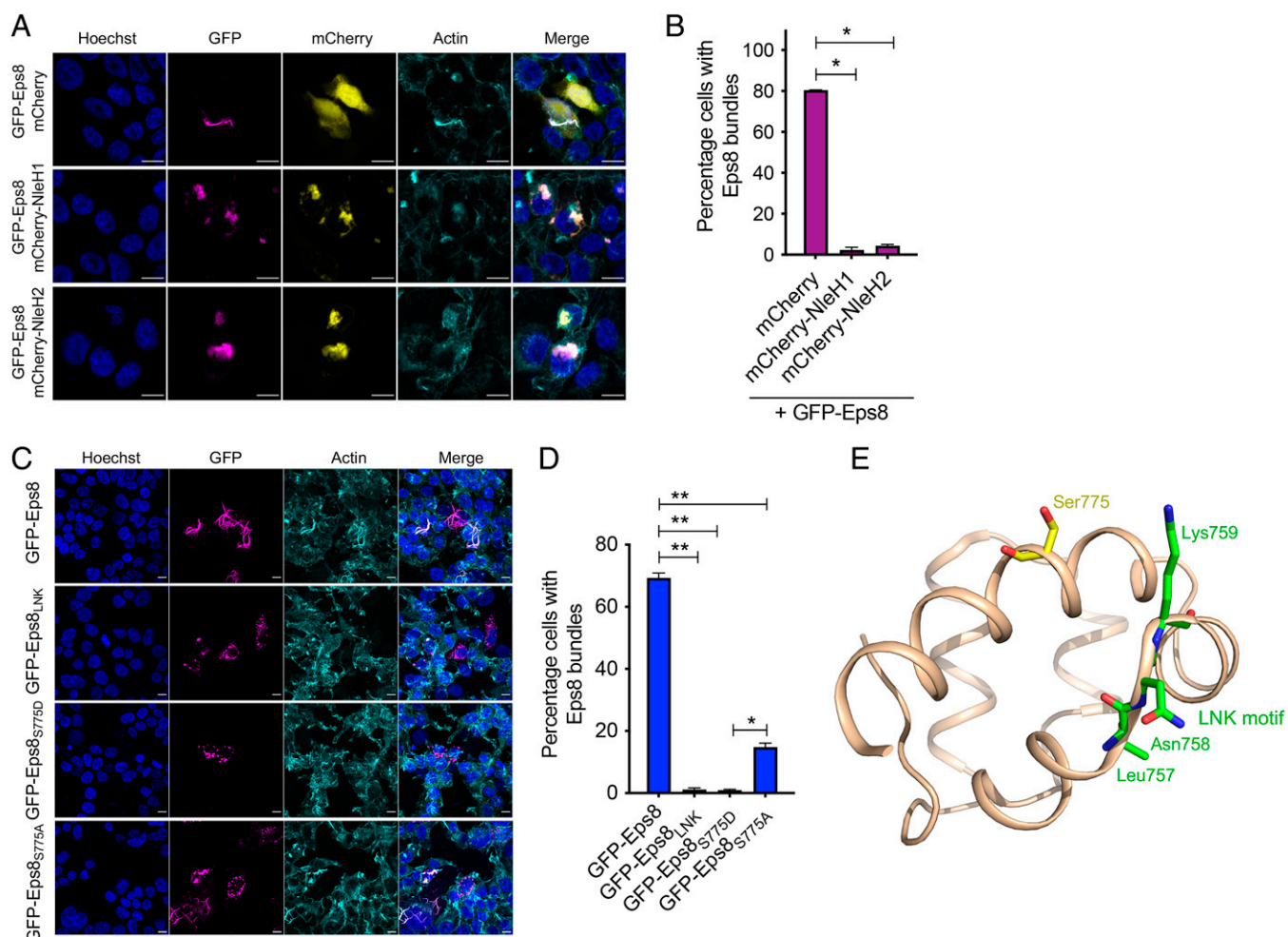

Fig. 4. NleH1 and NleH2 influence Eps8 bundling in transfected cells. *A.* Representative immunofluorescence fields of HEK292T cells cotransfected to express GFP-Eps8 (magenta) with mCherry, mCherry-NleH1, or mCherry-NleH2 (yellow). Hoechst and phalloidin were used to visualize cell nuclei (blue) and F-actin (cyan), respectively. Images are summation projections; scale bar represents 10 μm. *B.* Quantification of cotransfected HEK293T cells with GFP-Eps8 bundles as visualized by microscopic analysis. Results are mean + SEM percentage of cotransfected cells from three independent experiments, counting at least 40 cells per condition per experiment. *P < 0.0001, one-way ANOVA with Tukey's multiple comparisons test. *C.* Representative immunofluorescence fields of HEK293T cells transfected to express GFP-Eps8 derivatives (magenta). Hoechst and phalloidin were used to visualize cell nuclei (blue) and F-actin (cyan), respectively. Images are maximum intensity projections; scale bar represents 10 μm. *D.* Quantification of transfected HEK293T cells with GFP-Eps8 bundles as visualized by microscopic analysis. Results are mean + SEM percentage of transfected cells from three independent experiments, counting at least 100 cells per condition per experiment. *P = 0.0006, **P < 0.0001, one-way ANOVA with Tukey's multiple comparisons test. *E.* NMR structure of the C-terminal segment (residues 699–784) of Eps8 showing $_{757}$LNK$_{759}$ actin-bundling motif (green) and adjacent Ser$_{775}$ phosphorylation site (yellow) (PDB ID 2E8M). Ser775 is near Lys759 and, when phosphorylated, could form a salt bridge with the lysine, hijacking it from the LNK motif.

bundling activity, whereas the S775D phosphomimetic mutation completely inactivated bundling activity (Fig. 4 *C* and *D*). This suggested that Ser775 is important for Eps8 bundling activity, and its phosphorylation interrupts this activity. We then used the NMR structure of 699–784 segment of Eps8 (PDB ID: 2E8M) to map the location of Ser775 with respect to known functionally important residues. In the three-dimensional structure, we saw that Ser775 was located in an alpha helix adjacent to the $_{757}$LNK$_{759}$ motif, which is required for actin bundling (Fig. 4*E*).

In polarized intestinal epithelial cells, Eps8 localizes specifically to the apical tip of microvilli (25, 28, 29, 31). To investigate the effect of NleH1 and NleH2 on Eps8 localization during infection, we infected LS174T-W4 cells, a colonic epithelial cell line that undergoes polarization upon treatment with doxycycline (32). Consistent with previous reports, in uninfected polarized LS174T-W4 cells, Eps8 localized to the apical tips of microvilli (Fig. 5*A*) (29). In LS174-W4 cells

Fig. 5. Eps8 localization during EPEC infection. *A.* Super resolution microscopy imaging of endogenous Eps8 visualized using anti-Eps8 antibodies (magenta) in polarized LS174-W4 cells left uninfected or infected with wild-type EPEC E2348/69 or the Δ*nleH1*Δ*nleH2* double mutant for 3 h, expressing GFP (yellow). Phalloidin was used to visualize F-actin (cyan). Images are maximum intensity projections; scale bar represents 10 μm. *B.* Quantification of Eps8 localization with EPEC pedestals in polarized LS174-W4 cells infected with EPEC E2348/69 or derivatives for 3 h, as visualized by microscopic analysis shown in *SI Appendix,* Fig. S7. Results are mean + SEM percentage of infected cells from three independent experiments, counting at least 30 cells per condition, per experiment. *$P \leq 0.0001$, ns (not significant) compared to the percentage of E2348/69-infected cells showing Eps8 pedestal or dispersed localization, one-way ANOVA with Tukey's multiple comparisons test.

infected with wild-type EPEC, we observed a loss of brush border organization that was concomitant with actin accumulation beneath the site of bacterial attachment and loss of Eps8 microvillus staining (Fig. 5*A*). Although infection with EPEC Δ*nleH1*Δ*nleH2* also led to the characteristic actin accumulation beneath attached bacteria, we observed a striking enrichment of Eps8 at the site of bacterial attachment that was not evident during wild-type EPEC infection (Fig. 5*A*). Complementation of the double Δ*nleH1*Δ*nleH2* mutant with either NleH1 or NleH2 restored Eps8 dispersal from the site of bacterial attachment (Fig. 5*B* and *SI Appendix,* Fig. S7*A*). However, derivatives of NleH1 and NleH2 carrying mutations in both the catalytic site (KED) and PxxDY motifs were unable to complement the Δ*nleH1*Δ*nleH2* mutant (Fig. 5*B* and *SI Appendix,* Fig. S7*A*). Together these experiments suggested that NleH1 and NleH2 not only inhibit the bundling activity of Eps8 but influence the localization of Eps8 during EPEC infection by driving the dispersal of Eps8 from the AE lesion. During infection with the Δ*nleH1*Δ*nleH2* mutant, Eps8 appeared to sit above filamentous actin in the AE lesion (*SI Appendix,* Fig. S7*B*).

In summary, we found that the EPEC effector kinases NleH1 and NleH2 target the microvillus protein Eps8 for phosphorylation on Ser775. Interaction between the two proteins was mediated by noncanonical "proline-rich" motifs in NleH that bound to the SH3 domain of Eps8. Structural analysis showed that the PxxDY segment makes critical interactions with the SH3 domain of Eps8, placing the Pro in a hydrophobic pocket, forming hydrogen bonds with Glu and Tyr, and stacking interactions with Tyr. Residues outside of this pentapeptide provided additional interactions that together resulted in selectivity and high PxxDY–SH3 affinity, allowing NleH to compete with intracellular ligands of Eps8. In the absence of both NleH1 and NleH2, Eps8 remained within the pedestal of the EPEC AE lesion, suggesting that NleH-mediated redistribution of Eps8 is a pathogen-driven event. Hence, NleH1 and NleH2 may have a hitherto unrecognized role in the morphogenesis and composition of the EPEC AE lesion. One possibility is that NleH1 and NleH2 prevent the formation of new microvilli. Recent work has shown that formation of an Eps8/IRTKS complex at the cell surface is important for initiating microvillus growth and that loss of Eps8 from the complex leads to microvillus collapse (33). Further study of the role of Eps8 in AE lesion formation will aid our understanding of the roles of NleH1 and NleH2 during EPEC infection.
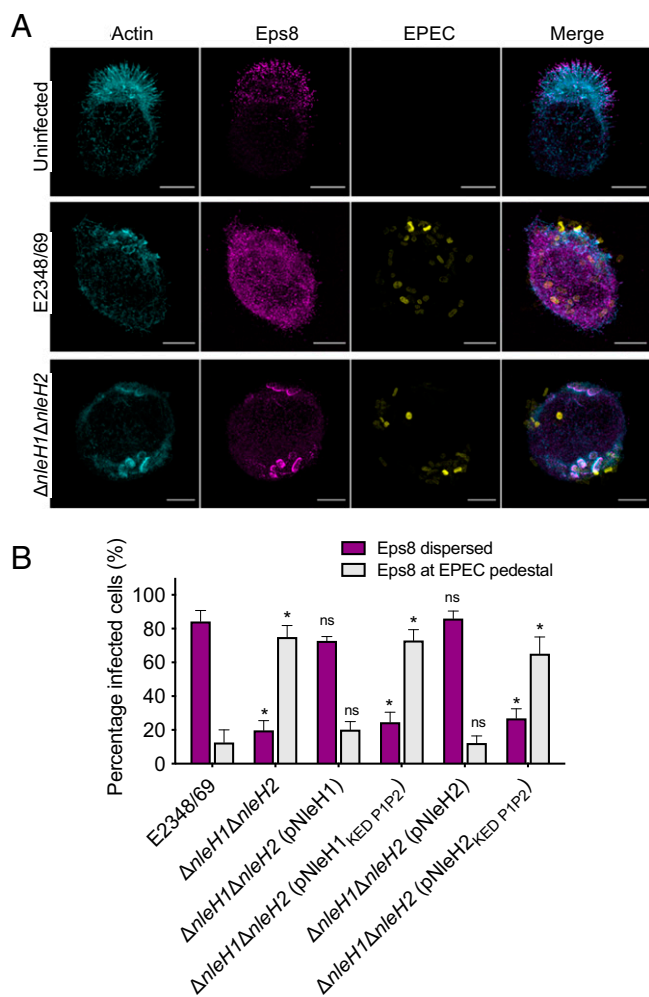
Materials and Methods

Bacterial Strains and Growth Conditions, DNA Cloning, and Purification. The bacterial strains, plasmids, and primers used in this study are listed in *SI Appendix,* Table S2. Bacteria were grown in Luria–Bertani (LB) broth at 37 °C with shaking or statically in Dulbecco's modified Eagle's medium GlutaMAX (DMEM; Life Technologies) at 37 °C with 5% CO_2 in the presence of ampicillin (100 μg/mL), kanamycin (100 μg/mL), or chloramphenicol (25 μg/mL) when required. EPEC E2348/69 genomic DNA was extracted with a *Quick*-DNA Miniprep kit (Zymo Research) according to the manufacturer's instructions. Human messenger RNA was extracted from HT-29 cells with TriSURE (Bioline) according to the manufacturer's protocol. Messenger RNA was deoxyribonuclease treated with Ambion DNaseI (Thermo Fisher Scientific) and then used as template for complementary DNA synthesis with the iScript complementary DNA synthesis kit (Bio-Rad). Site-directed mutagenesis was performed by amplifying specified DNA template with specified primers, followed by overnight digestion of template DNA with DpnI and transformation into XL1-blue *E. coli*. All sequences were verified with Sanger sequencing performed by the Australian Genome Research Facility or Micromon (Monash University) and analyzed in Sequencher 5.1 (Gene Codes Corporation).

Coimmunoprecipitation. HEK293T cells were seeded into 10-cm tissue culture dishes and cotransfected with 3 µg of one of pEGFP, pEGFP-NleH1, pEGFP-NleH2, or their respective PxxDY motif derivatives and 3 µg of pFlag-Eps8 or pFlag-Eps8$_{531-822}$. Cells were incubated for 16 h before being harvested for analysis. Cells were washed with cold phosphate-buffered saline (PBS) and lysed for 30 min with lysis buffer (50 mM Tris HCl pH 7.4, 150 mM NaCl, 1 mM ethylenediaminetetraacetic acid [EDTA], 1% Triton x-100, 10 mM NaF, 1 mM phenylmethylsulfonyl fluoride, 2 mM Na$_3$VO$_4$, with 1× EDTA-free Complete Protease Inhibitor Cocktail [Roche]). Cellular debris was pelleted by centrifugation, and lysates were subjected to immunoprecipitation with anti-FLAG M2 magnetic beads (Merck) according to the manufacturer's instructions. Briefly, supernatants were incubated with equilibrated anti-FLAG M2 magnetic beads at 4 °C for 3 h. Beads were washed with lysis buffer, and bound proteins were eluted by adding 3× FLAG peptide (100 µg/mL in lysis buffer; Merck) and incubating with rotation for a further 30 min. Eluates were magnetically separated from beads, and 4× lithium dodecyl sulfate (LDS) sample buffer (Thermo Fisher Scientific) supplemented with dithiothreitol (DTT) (50 mM) was added. Samples were boiled for 10 min before being subjected to PAGE and immunoblotting as described below.

PAGE and Immunoblotting. For analysis of cell monolayers, cells were lysed in cold lysis buffer (50 mM Tris·HCl pH 7.4, 150 mM NaCl, 1 mM EDTA, 1% Triton x-100, 10 mM NaF, 1 mM phenylmethylsulfonyl fluoride, 2 mM Na$_3$VO$_4$ with 1× EDTA-free Complete Protease Inhibitor Cocktail [Roche]). Cell lysates were pelleted, and equal volumes of supernatant were collected and added to 4× LDS sample buffer (Thermo Fisher Scientific) supplemented with DTT (50 mM), heated to 70 °C for 10 min, and resolved on 4–12% Bis-Tris Gels (Thermo Fisher Scientific) by PAGE. Protein gels were stained and visualized with Kangs Colloidal Coomassie blue or transferred to nitrocellulose membranes before being incubated for 1 h in 5% skim milk powder in Tris-buffered saline (TBS; 50 mM Tris·HCl pH 7.5, 150 mM NaCl) with 0.1% Tween 20. Membranes were washed and probed with one of the following primary antibodies diluted 1:1,000 in 5% bovine serum albumin (BSA) in TBS with 0.1% Tween 20: horseradish peroxidase (HRP)-conjugated monoclonal mouse anti-FLAG-M2 (Sigma-Aldrich), monoclonal rabbit anti-cleaved caspase-8 (Asp391)(18C8) (Cell Signaling Technology), polyclonal rabbit anti-cleaved caspase-3 (Asp175) (Cell Signaling Technology), monoclonal mouse anti-IκBα (L35A5) (Cell Signaling Technology), monoclonal mouse anti-GFP (7.1 and 13.1) (Roche), or monoclonal mouse anti-β-actin (Sigma-Aldrich) diluted 1:5,000. The secondary antibodies used were HRP-conjugated anti-mouse (Perkin-Elmer) and HRP-conjugated anti-rabbit (Perkin-Elmer) diluted 1:3,000 in TBS with 5% BSA and 0.1% Tween 20. Immunoblots were developed with Amersham ECL Western Blotting Detection Reagents (GE Healthcare) or Western Lightning Ultra (Perkin-Elmer), and chemiluminescence was detected with a DNR MF-ChemiBIS Bio-Imaging System or Amersham Imager 680.

Proteomic Sample Preparation. HT-29 cells were seeded into 10-cm tissue culture dishes 48 h before infection with EPEC derivatives. EPEC cultures grown by shaking overnight in LB were inoculated 1:100 into DMEM and subcultured for a further 3 h in 5% CO$_2$. Cells were infected with EPEC cultures at an optical density at 600 nm (OD$_{600}$) of 0.03 for 3 h. After infection cells were washed with ice cold PBS, lysed with GdmCl lysis buffer, and subjected to acetone precipitation (34). Precipitated protein was resuspended in digestion buffer (8 M urea, 100 mM ammonium bicarbonate [ABC], 20 mM DTT), and protein content was measured with a Pierce BCA Protein Assay Kit–Reducing Agent Compatible (Thermo Fisher Scientific). Samples were diluted to equal concentrations with digestion buffer prior and 1 mg of protein for each replicate alkylation with chloroacetamide (50 mM) for 60 min. The alkylation reaction was quenched with the addition of DTT (20 mM) and a further 15 min incubation. Samples were diluted with 4× volume of ABC (100 mM), then digested with trypsin (1:100 protein/protease ratio) overnight at 25 °C with shaking. Samples were acidified with formic acid prior to desalting with Sep-Pak C18 cartridges and dried to completion with a vacuum centrifuge.

Phosphopeptide Enrichment and MS Analysis. Titanium dioxide (TiO$_2$) enrichment of phosphopeptides was performed as described with minor alterations (35). Briefly, dried peptides were resuspended in loading buffer (1 M glycolic acid in 80% acetonitrile [ACN] and 5% trifluoroacetic acid [TFA]). TiO$_2$ resin (0.6 mg per 100 µg of peptide) (GL Sciences) was added and incubated with

shaking (2,000 rpm) for 10 min. Resin was pelleted by centrifugation (2,000 × g for 1 min) and supernatant transferred to a fresh tube. Additional TiO$_2$ (0.3 mg per 100 µg peptide) was added to the supernatant, incubated for 10 min with shaking, and pelleted as above. Supernatant was collected and dried to completion with a vacuum centrifuge to enable assessment of proteome-level changes. TiO$_2$ resin from the primary incubation was resuspended in loading buffer, then pooled with the secondary incubation resin. Resin was pelleted by centrifugation before being resuspended in wash buffer 1 (80% ACN, 1% TFA) and pelleted by centrifugation. Washing was repeated with wash buffer 2 (20% ACN, 0.2% TFA). To elute bound phosphopeptides, resin was subjected to two rounds of incubation with elution buffer (1% ammonium hydroxide, pH 11) for 15 min, followed by centrifugation to pellet resin and collection and pooling of supernatant. Eluate was dried to completion with a vacuum centrifuge. TiO$_2$ resin was regenerated by a round of washing with wash buffer 1, followed by a second wash with wash buffer 3 (50% ACN, 0.1% TFA). Dried peptides were resuspended in wash buffer 1 and incubated with shaking with regenerated TiO$_2$ resin for 10 min. Resin was pelleted by centrifugation, and supernatant was discarded before being washed with wash buffer 3. Two rounds of elution were repeated as described above, eluted peptide was acidified with the addition of formic acid. Eluted phosphopeptides and unbound peptides for total proteome analysis were desalted with C18 stage tips as described (36), with the addition of 1 mg of OLIGO R3 reverse phase resin (suspended in 100% ethanol; Thermo Fisher Scientific) for phosphopeptide samples before analysis by liquid chromatography mass spectrometry (LC-MS).

Identification of Phosphopeptides and Total Proteome from Complex Lysates Using Reversed Phase LC-MS. Phosphopeptide enrichments or total proteome inputs were resuspended in buffer A* (0.1% TFA, 2% ACN) and separated with a two-column chromatography setup comprising a PepMap100 C18 20 mm × 75 µm trap and a PepMap C18 500 mm × 75 µm analytical column (Thermo Fisher Scientific). Samples were concentrated onto the trap column at 5 µL/min for 5 min and infused into an Orbitrap Fusion Lumos Tribrid Mass Spectrometer (Thermo Fisher Scientific) at 300 nL/min via the analytical column with a Dionex Ultimate 3000 UPLC (Thermo Fisher Scientific). Total proteome input controls and label-free quantification (LFQ) phosphopeptide enrichment were separated via 210-min gradients, altering the buffer composition from 1% buffer B to 28% buffer B over 175 min, 28% buffer B to 40% buffer B over 10 min, and 40% buffer B to 100% buffer B over 2 min, then the composition was held at 100% buffer B for 3 min and then dropped to 3% buffer B over 5 min and held at 3% buffer B for another 15 min. The Lumos Mass Spectrometer was operated in a data-dependent mode, automatically switching between the acquisition of a single Orbitrap MS scan (120,000 resolution) every 3 s and Orbitrap high-energy collisional dissociation for each selected precursor (maximum fill time 60 ms, automatic gain control 2 × 10^5 with a resolution of 15,000 for Orbitrap tandem mass spectrometry [MS/MS] scans).

In Vitro in-Gel Digestion. In-gel tryptic digest was performed as previously described (37) with minor modifications. Following excision of proteins from polyacrylamide gels, gel slices were destained with wash buffer (50 mM ABC, 50% ethanol) for 20 min with shaking at 750 rpm, then washed with 100% ethanol and vacuum-dried. Gel slices were rehydrated with reduction buffer (10 mM DTT, 50 mM ABC) and incubated at 56 °C for 1 h with shaking, then washed twice with 100% ethanol. Samples were subsequently alkylated (55 mM iodoacetamide, 50 mM ABC) for 45 min at room temperature followed by two rounds of washing with wash buffer and two rounds of washing with 100% ethanol, then vacuum dried. Gel slices were then incubated with digestion buffer (20 µg/mL trypsin [Promega] in 50 mM ABC) for 1 h at 4 °C. Excess digestion buffer was removed, and gel slices were covered with 50 mM ABC and incubated at 37 °C for 16 h. After digestion, peptides were extracted from gel slices with extraction buffer (30% vol/vol ethanol, 3% vol/vol formic acid) and vacuum dried. Peptides were desalted with C18 stage tips as described (36), with the addition of 1 mg of OLIGO R3 reverse phase resin (suspended in 100% ethanol) before analysis by LC-MS.

Identification of Phosphopeptides from In Vitro Assays. Purified peptides were resuspended in Buffer A* and separated with a two-column chromatography setup comprising a PepMap100 C18 20 mm × 75 µm trap and a PepMap C18 500 mm × 75 µm analytical column (Thermo Fisher Scientific).

Samples were concentrated onto the trap column at 5 μL/min for 5 min and infused into an Orbitrap Fusion Lumos Tribrid Mass Spectrometer at 300 nl/min via the analytical column with a Dionex Ultimate 3000 UPLC (Thermo Fisher Scientific). Then 90-min gradients were run, altering the buffer composition from 1% buffer B to 28% buffer B over 60 min, 28% buffer B to 40% buffer B over 13 min, and 40% buffer B to 100% buffer B over 2 min, then the composition was held at 100% buffer B for 5 min and then dropped to 3% buffer B over 1 min and held at 3% buffer B for another 9 min. The Lumos Mass Spectrometer was operated in a data-dependent mode, automatically switching between the acquisition of a single Orbitrap MS scan (120,000 resolution) every 3 s and Orbitrap high-energy collisional dissociation for each selected precursor (maximum fill time 80 ms, automatic gain control 2×10^5 with a resolution of 30,000 for Orbitrap MS/MS scans).

MS Data Analysis. Identification of proteins and phosphorylated peptides was accomplished in MaxQuant (v1.5.3.1) (38). Searches were performed against the *E. coli* O127:H6 strain E2348/69 (Uniprot proteome ID UP000008205–*E. coli* O127:H6 strain E2348/69/EPEC, downloaded 28/07/2014, 4,595 entries) and the human (Uniprot proteome ID UP000005640–*Homo sapiens*, downloaded 24/10/2013, 84,843 entries) proteomes. Samples were searched with fixed modification of cysteine with carbamidomethylation, trypsin cleavage specificity allowing two missed cleavage events, and the variable modifications of oxidation of methionine, phosphorylation (Ser, Thr, Tyr), and acetylation of protein N-termini. To enhance the identification of peptides between samples, the Match between Runs option was enabled with a precursor match window set to 2 min and an alignment window of 10 min. For LFQ, the MaxLFQ option within MaxQuant (39) was enabled in addition to the requantification module. The resulting outputs were processed in the Perseus (v1.4.0.6) (40) analysis environment to remove reverse matches and common protein contaminants prior to further analysis. For identified phosphopeptides, only class I (localization >0.75) sites were considered for analysis and visualization. For LFQ comparisons, missing values were imputed with a standard derivation of 0.3σ and a downshift of 2.5σ in Perseus, with resulting data visualized with ggplot2 within R. All MS proteomics data have been deposited to the ProteomeXchange Consortium via the PRIDE partner repository (41) with the following dataset identifiers: label-free EPEC infection phosphopeptide enrichment PXD008480 and PXD031090, label-free EPEC infection total proteome PXD008481, and Eps8 in vitro kinase assay and in-gel digest PXD010925. All scripts and the Perseus processed data table used to generate figures are accessible in PRIDE (accession PXD031117).

Intact Molecular Weight Analysis. Protein molecular weights were obtained with an LTQ XL-Orbitrap hybrid mass spectrometer (Thermo Scientific). Samples were injected onto a PicoFrit fused silica capillary column (ProteoPepII, C18) with 100 μm inner diameter (300 Å, 5 μm; New Objective) attached to a nanoflow high-performance liquid chromatography (Easy-nLC II; Thermo Scientific) at 100% A and eluted at a 2% B/min gradient for 45 min (A, 4% acetonitrile + 0.2% formic acid; B, acetonitrile + 0.2% formic acid). Mass spectra were obtained at a resolution of 60,000 and *m/z* range of 400–1,800.

Yeast Two-Hybrid System Cotransformations. *Saccharomyces cerevisiae* Y2HGold was cotransformed with bait and prey plasmids via the lithium acetate method (42). Briefly, yeast were grown in yeast extract peptone dextrose supplemented with adenine broth overnight at 30 °C with shaking at 200 rpm. The overnight culture was inoculated into fresh yeast extract peptone dextrose supplemented with adenine at an OD_{600} of 0.2 and grown to an OD_{600} of 0.6–0.8. The culture was pelleted, resuspended in distilled water, then pelleted again. The culture was then resuspended in 100 mM lithium acetate and pelleted, and supernatant was removed. To the yeast pellet, polyethylene glycol (PEG 3500, 50% vol/vol) was added, followed by 1 M lithium acetate, salmon sperm DNA (2 mg/mL; Life Technologies), and 500 ng of each bait and prey plasmid. Pellets were mixed thoroughly before being incubated at 30 °C for 30 min, then heat shocked at 42 °C for 20 min. The yeast were pelleted then resuspended in distilled water before being plated onto selective media and incubated at 30 °C for 3–5 d.

In Vitro ATP-γS Kinase Assay. We incubated 5 μg of purified recombinant GST-Eps8₆₄₈₋₈₂₂ with 0.5 μg of purified recombinant His-NleH1^KD, His-NleH1^KD_KED, His-NleH2^KD, or His-NleH2^KD_KED in 30 μL of reaction buffer (40 mM Tris·HCl pH 7.5, 10 mM MgCl₂, 10 mM NaCl, 1 mM DTT, 1 mM ATP) at 37 °C for 3 h. Subsequently, 4× LDS sample buffer (Thermo Fisher) supplemented with DTT (50 mM) was added, and samples were heated to 70 °C for 10 min and subjected to PAGE as described below. Protein gels were stained with colloidal Coomassie blue protein stain (0.02% wt/vol Coomassie Brilliant Blue G-250, 5% wt/vol aluminum sulfate, 10% vol/vol ethanol, 2% vol/vol orthophosphoric acid). Bands of corresponding size to the protein of interest were excised from the gel and subjected to in-gel tryptic digest. For kinase assays followed by phosphorylation detection by Western blot, reactions were conducted via a protocol and novel chemistry developed by Allen and colleagues (16). We used ATP-γS instead of ATP, and phosphorylation was detected through an antibody hapten-mediated approach.

Reactions were conducted in 20 mM 4-(2-hydroxyethyl)-1-piperazineethanesulfonic acid (HEPES) 8.0, 200 mM NaCl, 10 mM MnCl₂ in a volume of 10 μL at room temperature, typically ranging in time between 30 and 60 min. Reactions were started by addition of ATP-γS to the final concentration of 0.1 mM and stopped by adding EDTA to a final concentration of 20 mM. NleH1 and NleH2, with their truncated derivatives 96–293 and 96–303 and kinase domains 128–293 and 140–303, respectively, were used at concentrations of 0.1–1 μg/10 μL of the reaction mixture, while the substrates, Eps8(531–822) and Eps8(648–822), were added to yield 1 μg/10 μL of the reaction volume. After stopping, the reactions were treated with an alkylating agent paranitrobenzyl mesylate (Abcam) by adding the latter to 2.5 mM final concentration and letting the reaction proceed for 2 h at room temperature or overnight at 4 °C. The resulting thiophosphate ester hapten in lieu of phosphorylation sites was detected by rabbit monoclonal anti–thiophosphate ester antibody (Abcam) and goat anti-rabbit HRP-conjugated secondary antibodies in Western blot.

Confocal and Super Resolution Microscopy. To visualize Eps8 localization in nonpolarized cells, HEK293T cells were seeded onto coverslips in 24-well tissue culture trays 24 h before being cotransfected with 0.4 μg pmCherry, pmCherry-NleH1, pmCherry-NleH2, or derivatives and 0.4 μg pEGFP-Eps8. Following transfection, cells were incubated for a further 16 h at 37 °C and 5% CO₂ before being fixed with paraformaldehyde (PFA) (4% in PBS) for 15 min at room temperature. PFA was removed, and cells were washed thoroughly with PBS before being incubated for 1 h with Hoechst (2.4 μg/mL; Thermo Fisher) and Alexa Fluor-647 conjugated phalloidin (diluted 1:500; Invitrogen) diluted in 3% BSA in PBS. To visualize the localization of Eps8 derivatives, HEK293T cells were seeded onto coverslips in 24-well tissue culture trays 24 h prior to being cotransfected with 0.4 μg pEGFP-Eps8, pEGFP-Eps8_S775D, pEGFP-Eps8_S775A, or pEGFP-Eps8_L757A-K759A. Cells were incubated for 24 h prior to being fixed with PFA (4% in PBS) for 15 min, followed by thorough washing with PBS. Cells were incubated for a further 15 min in PBS with Hoechst (2.4 μg/mL; Thermo Fisher) to stain DNA and phalloidin–tetramethylrhodamine B isothiocyanate (diluted 1:2,000; Sigma) to stain F-actin. Coverslips were mounted onto microscope slides with Prolong Gold Antifade Reagent (Invitrogen), and images were acquired with a Nikon C1 or Olympus FV1200 confocal laser scanning microscope. For quantitation of cells with Eps8 bundles, coverslips were blinded and then imaged with a Nikon C1 confocal laser scanning microscope. All transfected cells per field of view were counted, with a minimum of 40 cells (cotransfection experiment) or 100 cells (Eps8 mutant experiment) counted per condition for three replicates.

To visualize Eps8 localization during EPEC infection of polarized epithelial cells, LS174T-W4 cells were seeded onto coverslips in six-well tissue culture trays and treated with doxycycline (1 μg/mL) to induce polarization. After 16 h, cells were infected with EPEC. EPEC cultures were grown by shaking overnight in LB, subcultured for 8 h in LB, then inoculated 1:500 into DMEM and grown overnight at 37 °C in 5% CO₂ without shaking. LS174T-W4 cells were left uninfected or infected with EPEC derivatives at an OD_{600} of 0.04. After 2.5 h, cells were washed with warm PBS and fixed with warm PFA (4% in PBS) for 15 min at 37 °C, followed by thorough washing with PBS. Cells were permeabilized with 0.1% Triton X-100 (diluted in PBS) for 15 min before PBS washing and then blocked in 3% BSA (in PBS) for 1 h at 37 °C. Coverslips were incubated for 1 h at 37 °C with monoclonal mouse anti-Eps8 (BD Biosciences) diluted 1:400 in 1% BSA in PBS. Following PBS washes, coverslips were incubated with goat anti-mouse immunoglobulin G (IgG) Alexa Fluor-568 conjugated antibody (diluted 1:2,000; Invitrogen) and Alexa Fluor-647 conjugated phalloidin (diluted 1:500;

Invitrogen) in 1% BSA in PBS for 45 min at room temperature. Coverslips were mounted onto microscope slides with Prolong Gold Antifade Reagent (Thermo Fisher), and superresolution microscopy images were acquired with a Zeiss Elyra LSM880 with AiryScan and subjected to Huygens deconvolution. For experiments involving complemented EPEC mutants, LS174T-W4 cells were seeded and infected as above, except that 1 h before infection, DMEM cultures of EPEC were induced with 1 mM isopropyl β-D-1-thiogalactopyranoside, and infection time was 3.5 h. Coverslips were incubated for 1 h at 37 °C with monoclonal mouse anti-Eps8 (BD Biosciences) diluted 1:400 and rabbit polyclonal anti-O127 LPS (Statens Serum Institut) diluted 1:600 in 1% BSA in PBS. Coverslips were incubated with the following secondary antibodies or reagents: goat anti-mouse IgG Alexa Fluor-568 conjugated antibody (diluted 1:2,000; Invitrogen), goat anti-rabbit IgG Alexa Fluor-488 conjugated antibody (diluted 1:2,000; Invitrogen), and Alexa Fluor-647 conjugated phalloidin (diluted 1:500; Invitrogen). For quantitation, coverslips were blinded and imaged with a Nikon C1 confocal laser scanning microscope. All infected cells per field of view were counted, with a minimum of 30 cells counted per condition for three replicates.

Multiangle Light Scattering. The molecular weight of Eps8(531–591) was estimated via multiangle light scattering. Gel filtration of purified proteins was performed with the output from the Superdex 200 column connected to a triple-angle light scattering instrument miniDAWN TREOS (Wyatt Technology Corporation) and refracting index measurement instrument Optilab rEX (Wyatt Technology Corporation). The proteins' molecular weight was estimated with BSA as a control and Wyatt's ASTRA software.

Isothermal Titration Calorimetry. Purified proteins were concentrated and dialyzed overnight against 20 mM HEPES 8.0, 200 mM NaCl, 0.5 mM tris(2-carboxyethyl)phosphine at 4 °C overnight. Next day, the proteins and the buffer were degassed and applied to trials with a Nano ITC calorimeter (TA Instruments). Proteins to be used in the syringe were concentrated to 400 μM–1 mM, while the concentration of the proteins in the cell was 40–100 μM. A typical isothermal titration calorimeter protocol included 20 injections of 2.5 μL per injection into a 250-μL volume cell with 250 s between injections at 20 °C. Control experiments included titrating the protein in the syringe into the buffer. For affinity determination between Eps8(648–822) and NleH2(140–303), Eps8 was used in the syringe at 2.43 mM concentration, while 0.169 mM NleH2 was in the cell. Buffer for dialysis was 50 mM HEPES 8.0, 200 mM NaCl, 0.25 mM tris(2-carboxyethyl)phosphine, 0.5 mM benzamidine, 1 mM $MgCl_2$. Adenylyl-imidodiphosphate was added to the solutions of Eps8 and NleH2 and buffer after dialysis to a final concentration of 0.35 mM.

Eps8 SH3 Domain Crystallization. Eps8 SH3 domain was concentrated to around 20 mg/mL, mixed with NleH1 peptide, covering the second SH3 motif PPELPSVDYNSL (aa 121–132) (GenScript) at 3 mM final concentration, and applied for crystallization screening. Sea urchin–looking crystals grew in the presence of 35% PEG 8,000. The crystals were reproduced in a 1-μL hanging drop in a 24-well crystallization plate, upon which they changed their morphology to plates. The crystals were transferred to 40% PEG 8,000, used as a cryoprotectant, and frozen in liquid nitrogen. The diffraction datasets were obtained on the Canadian Macromolecular Crystallography Facility–Bending Magnet beamline of the Canadian Light Source, equipped with a bending magnet, double-multilayer monochromator, ACCEL MD2 microdiffractometer, and Pilatus3 S 6M X-ray detector. The data were processed with XDSGO script, available at the Canadian Light Source, to a resolution of 1.43 Å (*SI Appendix*, Table S1). The structure was solved by molecular replacement with Phazer, using mouse Eps8 SH3

monomeric domain structure (PDB ID 1I0C). The differences between the mouse and the human SH3 domains were manually corrected, and the NleH1 second DY motif was manually built into the empty electron density.

Eps8 Bioinformatical Analysis. The protein sequences of Eps8 (accession number Q12929), Eps8L1 (accession number Q8TE68), and Eps8L2 (accession number Q9H6S3) were aligned in Clustal Omega (43). The NMR structure of Eps8 (residues 699–784) was accessed from the PDB database (PDB ID: 2E8M) (44) and visualized in Jmol (jmol.sourceforge.net).

Extended Materials and Methods. Extended materials and methods including detailed information on expression vector cloning, construction of bacterial mutants, construction of inducible cell lines expressing NleH, recombinant protein purification, and dual luciferase assays are provided as *SI Appendix*.

Author affiliations: [a]Centre for Innate Immunity and Infectious Diseases, Hudson Institute of Medical Research, Clayton, VIC 3168, Australia; [b]Department of Molecular and Translational Science, Monash University, Clayton, VIC 3168, Australia; [c]Department of Microbiology and Immunology, University of Melbourne at the Peter Doherty Institute for Infection and Immunity, Melbourne, VIC 3000, Australia; [d]Department of Biochemistry, Microbiology and Immunology, University of Saskatchewan, Saskatoon, SK S7N 5E5, Canada; [e]Biological Optical Microscopy Platform and Department of Biochemistry & Pharmacology, Faculty of Medicine, Dentistry and Health Sciences, The University of Melbourne, Melbourne, VIC 3010, Australia; [f]Department of Cell and Developmental Biology, University Medical Center, Vanderbilt University School of Medicine, Nashville, TN; and [g]Department of Microbiology, Monash University, Clayton, VIC 3168, Australia

1. K. L. Kotloff *et al.*, Burden and aetiology of diarrhoeal disease in infants and young children in developing countries (the Global Enteric Multicenter Study, GEMS): A prospective, case-control study. *Lancet* **382**, 209–222 (2013).
2. G. Frankel, A. D. Phillips, Attaching effacing *Escherichia coli* and paradigms of Tir-triggered actin polymerization: Getting off the pedestal. *Cell. Microbiol.* **10**, 549–556 (2008).
3. A. R. Wong *et al.*, Enteropathogenic and enterohaemorrhagic *Escherichia coli*: Even more subversive elements. *Mol. Microbiol.* **80**, 1420–1438 (2011).
4. E. Martinez *et al.*, Binding to Na(+) /H(+) exchanger regulatory factor 2 (NHERF2) affects trafficking and function of the enteropathogenic *Escherichia coli* type III secretion system effectors Map, EspI and NleH. *Cell. Microbiol.* **12**, 1718–1731 (2010).
5. A. M. Grishin *et al.*, NleH defines a new family of bacterial effector kinases. *Structure* **22**, 250–259 (2014).
6. C. Hemrajani *et al.*, NleH effectors interact with Bax inhibitor-1 to block apoptosis during enteropathogenic *Escherichia coli* infection. *Proc. Natl. Acad. Sci. U.S.A.* **107**, 3129–3134 (2010).
7. X. Gao *et al.*, Bacterial effector binding to ribosomal protein s3 subverts NF-kappaB function. *PLoS Pathog.* **5**, e1000708 (2009).
8. S. V. Royan *et al.*, Enteropathogenic E. coli non-LEE encoded effectors NleH1 and NleH2 attenuate NF-κB activation. *Mol. Microbiol.* **78**, 1232–1245 (2010).
9. F. Wan *et al.*, IKKβ phosphorylation regulates RPS3 nuclear translocation and NF-κB function during infection with Escherichia coli strain O157:H7. *Nat. Immunol.* **12**, 335–343 (2011).
10. T. H. Pham *et al.*, Functional differences and interactions between the Escherichia coli type III secretion system effectors NleH1 and NleH2. *Infect. Immun.* **80**, 2133–2140 (2012).
11. T. H. Pham, X. Gao, G. Singh, P. R. Hardwidge, Escherichia coli virulence protein NleH1 interaction with the v-Crk sarcoma virus CT10 oncogene-like protein (CRKL) governs NleH1 inhibition of the ribosomal protein S3 (RPS3)/nuclear factor κB (NF-κB) pathway. *J. Biol. Chem.* **288**, 34567–34574 (2013).
12. M. Yadav *et al.*, Binding specificity of type three secretion system effector NleH2 to multi-cargo chaperone CesT and their phosphorylation. *Protein Sci.* **30**, 2433–2444 (2021).

13. K. S. Robinson *et al.*, The enteropathogenic *Escherichia coli* effector NleH inhibits apoptosis induced by *Clostridium difficile* toxin B. *Microbiology (Reading)* **156**, 1815–1823 (2010).
14. N. Offenhäuser *et al.*, The eps8 family of proteins links growth factor stimulation to actin reorganization generating functional redundancy in the Ras/Rac pathway. *Mol. Biol. Cell* **15**, 91–98 (2004).
15. G. Scita *et al.*, An effector region in Eps8 is responsible for the activation of the Rac-specific GEF activity of Sos-1 and for the proper localization of the Rac-based actin-polymerizing machine. *J. Cell Biol.* **154**, 1031–1044 (2001).
16. J. J. Allen *et al.*, A semisynthetic epitope for kinase substrates. *Nat. Methods* **4**, 511–516 (2007).
17. A. M. Mongioví *et al.*, A novel peptide-SH3 interaction. *EMBO J.* **18**, 5300–5309 (1999).
18. O. Aitio *et al.*, Structural basis of PxxDY motif recognition in SH3 binding. *J. Mol. Biol.* **382**, 167–178 (2008).
19. K. Richter *et al.*, Small molecule AX-024 reduces T cell proliferation independently of CD3ε/Nck1 interaction, which is governed by a domain swap in the Nck1-SH3.1 domain. *J. Biol. Chem.* **295**, 7849–7864 (2020).
20. K. V. Kishan, M. E. Newcomer, T. H. Rhodes, S. D. Guilliot, Effect of pH and salt bridges on structural assembly: Molecular structures of the monomer and intertwined dimer of the Eps8 SH3 domain. *Protein Sci.* **10**, 1046–1055 (2001).
21. K. V. Kishan, G. Scita, W. T. Wong, P. P. Di Fiore, M. E. Newcomer, The SH3 domain of Eps8 exists as a novel intertwined dimer. *Nat. Struct. Biol.* **4**, 739–743 (1997).
22. T. Kesti *et al.*, Reciprocal regulation of SH3 and SH2 domain binding via tyrosine phosphorylation of a common site in CD3epsilon. *J. Immunol.* **179**, 878–885 (2007).
23. K. Takeuchi *et al.*, Structural and functional evidence that Nck interaction with CD3epsilon regulates T-cell receptor activity. *J. Mol. Biol.* **380**, 704–716 (2008).
24. A. Disanza *et al.*, Eps8 controls actin-based motility by capping the barbed ends of actin filaments. *Nat. Cell Biol.* **6**, 1180–1188 (2004).
25. A. Croce *et al.*, A novel actin barbed-end-capping activity in EPS-8 regulates apical morphogenesis in intestinal cells of Caenorhabditis elegans. *Nat. Cell Biol.* **6**, 1173–1179 (2004).
26. A. Disanza *et al.*, Regulation of cell shape by Cdc42 is mediated by the synergic actin-bundling activity of the Eps8-IRSp53 complex. *Nat. Cell Biol.* **8**, 1337–1347 (2006).
27. M. Hertzog *et al.*, Molecular basis for the dual function of Eps8 on actin dynamics: Bundling and capping. *PLoS Biol.* **8**, e1000387 (2010).
28. A. Tocchetti *et al.*, Loss of the actin remodeler Eps8 causes intestinal defects and improved metabolic status in mice. *PLoS One* **5**, e9468 (2010).
29. M. M. Postema, N. E. Grega-Larson, A. C. Neininger, M. J. Tyska, IRTKS (BAIAP2L1) elongates epithelial microvilli using EPS8-dependent and independent mechanisms. *Curr. Biol.* **28**, 2876–2888.e4 (2018).
30. J. Roffers-Agarwal, J. B. Xanthos, J. R. Miller, Regulation of actin cytoskeleton architecture by Eps8 and Abi1. *BMC Cell Biol.* **6**, 36 (2005).
31. L. M. Meenderink *et al.*, Actin dynamics drive microvillar motility and clustering during brush border assembly. *Dev. Cell* **50**, 545–556.e4 (2019).
32. A. F. Baas *et al.*, Complete polarization of single intestinal epithelial cells upon activation of LKB1 by STRAD. *Cell* **116**, 457–466 (2004).
33. I. M. Gaeta, L. M. Meenderink, M. M. Postema, C. S. Cencer, M. J. Tyska, Direct visualization of epithelial microvilli biogenesis. *Curr. Biol.* **31**, 2561–2575.e6 (2021).
34. S. J. Humphrey, S. B. Azimifar, M. Mann, High-throughput phosphoproteomics reveals in vivo insulin signaling dynamics. *Nat. Biotechnol.* **33**, 990–995 (2015).
35. K. Engholm-Keller, M. R. Larsen, Improving the phosphoproteome coverage for limited sample amounts using TiO2-SIMAC-HILIC (TiSH) phosphopeptide enrichment and fractionation. *Methods Mol. Biol.* **1355**, 161–177 (2016).
36. J. Rappsilber, M. Mann, Y. Ishihama, Protocol for micro-purification, enrichment, pre-fractionation and storage of peptides for proteomics using StageTips. *Nat. Protoc.* **2**, 1896–1906 (2007).
37. A. Shevchenko, H. Tomas, J. Havlis, J. V. Olsen, M. Mann, In-gel digestion for mass spectrometric characterization of proteins and proteomes. *Nat. Protoc.* **1**, 2856–2860 (2006).
38. J. Cox, M. Mann, MaxQuant enables high peptide identification rates, individualized p.p.b.-range mass accuracies and proteome-wide protein quantification. *Nat. Biotechnol.* **26**, 1367–1372 (2008).
39. J. Cox *et al.*, Accurate proteome-wide label-free quantification by delayed normalization and maximal peptide ratio extraction, termed MaxLFQ. *Mol. Cell. Proteomics* **13**, 2513–2526 (2014).
40. S. Tyanova *et al.*, The Perseus computational platform for comprehensive analysis of (prote)omics data. *Nat. Methods* **13**, 731–740 (2016).
41. J. A. Vizcaíno *et al.*, 2016 update of the PRIDE database and its related tools. *Nucleic Acids Res.* **44**, 11033 (2016).
42. R. D. Gietz, R. H. Schiestl, A. R. Willems, R. A. Woods, Studies on the transformation of intact yeast cells by the LiAc/SS-DNA/PEG procedure. *Yeast* **11**, 355–360 (1995).
43. F. Sievers *et al.*, Fast, scalable generation of high-quality protein multiple sequence alignments using Clustal Omega. *Mol. Syst. Biol.* **7**, 539 (2011).
44. H. Berman, K. Henrick, H. Nakamura, Announcing the worldwide Protein Data Bank. *Nat. Struct. Biol.* **10**, 980 (2003).
45. Y. Perez-Riverol *et al.*, The PRIDE database resources in 2022: a hub for mass spectrometry-based proteomics evidences. *Nucleic Acids Res.* **50**, D543–D552 (2022).
46. N. Scott, E. Hartland, NleH LFQ phoshoproteome analysis. PRIDE. https://www.ebi.ac.uk/pride/archive/projects/PXD008480. Deposited 18 December 2017.
47. N. Scott, E. Hartland, NleH LFQ phoshoproteome analysis (EThcD runs). PRIDE. https://www.ebi.ac.uk/pride/archive/projects/PXD031090. Deposited 19 January 2022.
48. N. Scott, E. Hartland, Input control proteome analysis of EP EC infection (LFQ). PRIDE. https://www.ebi.ac.uk/pride/archive/projects/PXD008481. Deposited 18 December 2017.
49. N. Scott, E. Hartland, Esp8 in viro assay. PRIDE. https://www.ebi.ac.uk/pride/archive/projects/PXD010925. Deposited 29 August 2018.
50. N. Scott, E. Hartland, NleH1/2 proteomic analysis scripts. PRIDE. https://www.ebi.ac.uk/pride/archive/projects/PXD031117. Deposited 20 January 2022.